Astron. Astrophys. 358, 1007–1021 (2000)

ASTRONOMY AND ASTROPHYSICS

AR Lacertae: Hα chromospheric emission and radial velocities from long-term optical spectroscopy*

A. Frasca[1], **G. Marino**[2], **S. Catalano**[1], **and E. Marilli**[1]

[1] Osservatorio Astrofisico di Catania, Via S. Sofia 78, 95125 Catania, Italy
[2] Istituto di Astronomia, Università di Catania, Viale Andrea Doria 6, 95125 Catania, Italy

Received 8 April 1999 / Accepted 27 April 2000

Abstract. We present here the results of spectroscopic studies in the Hα region of the active eclipsing binary AR Lac (G2IV+K0IV) obtained at Catania Astrophysical Observatory in 1989, 1990, 1994, 1996 and 1997. Accurate measurements of radial velocities by using the cross-correlation method have been made and a new orbital solution has been derived. The equivalent width of the Hα emission core has been measured by subtraction of spectra synthesised from standard non-active stars of spectral types similar to those of the two components. We find chromospheric emission from both components in most of the spectra. No rotational modulation of the Hα emission is apparent. The absorption excess observed near and during primary minima in 1997 is interpreted as the effect of a prominence-like structure anchored between the leading and the trailing hemisphere of the cool component. This interpretation is fully compatible with the radial velocities of the Hα emission peaks in the subtracted spectra.

The observation of a Hα flare in 1989 on the cool star is also reported and an estimate of the size of the magnetic structure involved in the event is proposed.

Key words: stars: activity – stars: binaries: eclipsing – stars: binaries: spectroscopic – stars: individual: AR Lac

1. Introduction

The totally eclipsing binary AR Lacertae (HD 210334, BD +45° 3813) is a well known RS CVn double-lined system whose components, a G2 IV and a K0 IV star, show signatures of an intense solar-like activity (see eg. Lanza et al. 1998 and references therein).

Emissions in the Ca II H & K lines were first observed by Sanford (1951) and more recent spectra, obtained by Bopp (1983) and Fernández-Figueroa et al. (1994), gave evidence for emission cores in the lines of both components. The double emission in the Mg II h & k lines clearly confirms that both stars are chromospherically active and show that discrete plage regions are resolvable on the K star surface (Walter et al. 1983, Neff et al. 1989). Recent analyses of Mg II h & k lines, from IUE observations, partially summarized in Neff (1992) and in Pagano et al. (1994), show that the discrete plages on the K star migrate in longitude and latitude. The Mg II emission flux of the G2 IV component was found almost constant from 1981 to 1991 while that of the K0 IV star showed a maximum around 1986–1987. No smooth rotational modulation of the line integrated flux has been found, but both stars generally appear brighter in their trailing hemispheres than in their leading ones.

Spatial correlation between photospheric and chromospheric active regions has been clearly seen only in 1989 and it is doubtful in other occasions (Pagano, 1993). Moreover, the spectral imaging analysis performed by Pagano (1993) suggested a relatively steady chromospheric active region close to the substellar point of the K star. Such conclusion is in general agreement with X-ray observations (Ottmann et al. 1993, Siarkowski et al. 1996) as well as with the photospheric maps of Lanza et al. (1998).

AR Lac ($P_{orb} \sim 1.983$) shows an out-of-eclipse photometric wave in the optical bands interpreted as starspots modulation. Information on geometric and physical parameters of the spots can be safely derived in the case of eclipsing binaries, because of the good knowledge of the system inclination. Thanks also to the scanning of the stellar disks during the eclipses, additional information on the latitude and size of the spots can be derived. The light curve solution made by Lanza et al. (1998) supports the existence of compact starspots on the G2 IV primary star and a sector structure of the active longitudes on the K0 IV secondary star. In the same work evidence for preferential active longitudes, long term spots' migration and variations of the spots' distribution were given. The existence of an activity cycle was also confirmed.

Out-of-eclipse variation of emission is well observed at radio wavelengths (Lefèvre et al. 1994), and X-ray (Ottmann & Schmitt 1994; Strassmeier et al. 1993). A huge X–ray flare, consisting of multiple events and with a total duration of about 4 days, was detected by ROSAT observations (Ottman & Schmitt 1994).

Extensive Hα observations of AR Lac in 1976 and 1977 by Bopp & Talcott (1978) show large changes in the absorption EW up to a factor of three, and some filling in the Hα profile

Send offprint requests to: A. Frasca (afr@sunct.ct.astro.it)

* Based on observations collected at the Catania Astrophysical Observatory, Italy

of the cooler component during the giant radio flare observed by Feldman (1978), during which the received flux raised from undetectable levels up to 500 mJy. Large changes in the Hα line depth were also observed by Nations & Ramsey (1980). They displayed spectra showing, at second quadrature, a strong deepening of the Hα line of the G2 component, which became deeper than that of the secondary one, whose depth appeared to be unchanged.

From difference Hα profiles, derived by subtracting synthetic spectra, Huenemoerder & Ramsey (1984) found no definite emission from either component, with the exception of only few cases. Liu & Tan (1986) reported on variability of Hα line. They measured equivalent widths smaller than those of normal inactive standard stars, thus indicating spectra filled in by emission.

Frasca & Catalano (1994), comparing spectra at 0.9 Å resolution with synthetic ones, were able to separate the emission filling the Hα photospheric profile of both stars in all observations obtained very close to the quadratures. Also Montes et al. (1995) found excess Hα emission from both components.

Recently, Hall and Wolowitz (1998), analysing a consistent data set of Hα spectra, showed a variable excess Hα emission of both components of AR Lac with a more prominent variation of the K0 IV component on rotational, fixed-phase and long-term time scales.

Although AR Lac is a very well-studied RS CVn star, there are very few determinations of orbital and physical parameters from radial velocity measurements. This because, the orbital period of this system is almost exactly 2 days and it is very difficult to achieve a good phase coverage during an observational run. The only published solutions are those by Harper (1933) and Sanford (1951). The latter have been revised by Popper (1980, 1990). Recently Gunn et al. (1998) determined new radial velocities but values are clustered around two specific phases.

Here we analyse and discuss our spectroscopic observations of AR Lac, in a spectral region including the Hα line and several photospheric lines of interest, performed in recent years at Catania Observatory. Spectra were obtained with the aim of getting new radial velocity measurements well distributed in phase, investigating in more detail the Hα emission excess and its nature, studying the chromospheric level variation both on short and long time-scales, searching for rotational modulation indicative of chromospheric inhomogeneities, and determining new spectroscopic elements.

We also re-analyse and discuss the low resolution spectra which were partially used in Frasca & Catalano (1994) for a Hα statistical study of RS CVn systems and other unpublished low-resolution spectra acquired in 1990. We furthermore analyse the Hα flare detected in 1989.

Some issues regarding the analysis techniques are critically discussed in connection with the obtained results.

2. Observations and data reduction

The observations have been performed with the échelle spectrograph at the 91-cm telescope of the Catania Astrophysical Observatory *M. G. Fracastoro* station in 1989, 1990, 1994, 1996 and 1997. We used the instrumental apparatus in two different configurations and with two different detectors:

- In the years 1989, 1990 we used the spectrograph in low-dispersion mode with the 1200 lines/mm échellette grating which gives a linear dispersion of 40 Å/mm. The spectra were recorded on a front-illuminated 385×576 E. E. V. CCD of $22\times22\ \mu m$ pixel-size. In this configuration the one-pixel resolution was 0.89 Å. The slit width of $150\ \mu m$ we used, yields a projected half-width spectral element of 0.9 Å on the focal plane. The size of CCD allowed a wavelength coverage of about 450 Å. In these seasons the spectrograph was directly attached to the telescope Cassegrain focus.
- In the years 1994, 1996 and 1997 we used the échelle cross-dispersion configuration obtaining a resolution of about 0.46 Å, as deduced from the FWHM of the Th–Ar calibration lamp. The spectrograph was fed by the telescope through an optical fiber (UV - NIR, $200\ \mu m$ core diameter) and was placed in a stable position in the room below the dome level. In 1994 the camera was equipped with the same CCD detector of the low-resolution mode. Since 1996 a new front-illuminated CCD with 800×1152 pixels (pixel size of $22.5\ \mu m$) has being used. With the last larger CCD we were able to record four orders in each frame, spanning from about 6050 to 6650 Å, and nearly completely covering each échelle order.

The signal-to-noise ratio (S/N) attained in the low dispersion configuration was about 100-150 at the continuum near the Hα line. In the high resolution spectra the S/N ratio varied from about 40 to about 150 due to the highly variable weather conditions during the observation seasons.

To perform radial velocity determinations and spectral synthesis analysis, in addition to the program stars we observed many "normal" stars, considered inactive, or much less active than RS CVn binaries, and radial velocity standard stars.

The data reduction was performed by using the ECHELLE task of IRAF[1] package following the standard steps: background subtraction, division by a flat field spectrum given by a halogen lamp, wavelength calibration using the emission lines of Cesium (for low-resolution only) and Thorium-Argon lamps, normalisation to the continuum through a polynomial fit.

Major telluric lines are clearly identified in the spectra as instrumental width features on the continuum and along the rotationally broadened lines of AR Lac (as shown in Fig. 4). They were interactively eliminated by a simple linear interpolation while performing the cross-correlation analysis for the radial velocity determinations (see next section).

The most disturbing line for our analysis of the Hα emission is the H_2O line at λ 6564.206 (Moore et al. 1966). It is barely visible in our spectra (see Fig. 4) and its expected contribution

[1] IRAF is distributed by the National Optical Astronomy Observatory, which is operated by the Association of University for Research in Astronomy, inc. (AURA) under cooperative agreement with the National Science Foundation.

to the Hα emission evaluation, as we will discuss in Sect. 6, is negligible.

3. Radial velocities and orbital solution

The large number of high-resolution spectra, acquired in different years, has allowed us to determine a new more accurate orbital solution. Radial-velocity determinations have been made by means of the cross-correlation method using the IRAF task FXCOR (see eg. Tonry & Davis 1979, Fitzpatrick 1993). This cross-correlation technique has been widely used to determine stellar radial velocities (e.g. Simkin 1974, Gunn et al. 1996). The high-resolution AR Lac spectra have been compared with spectra of the bright slow-rotating stars ϵ Cyg and α Ari, whose radial velocities are $-10.6\,\mathrm{km\,s^{-1}}$ and $-14.3\,\mathrm{km\,s^{-1}}$ respectively (Evans, 1967). Template spectra of these reference stars were obtained systematically during all the observing runs. To test the reliability of ϵ Cyg and α Ari as standard radial-velocity stars, and the performances of our spectrograph, we made cross-correlations of their spectra with those of other primary RV standard stars observed from time to time. From these measurements we obtain an average accuracy of ± 0.4 km s^{-1} r.m.s. which is well within the limits given by the spectral resolution and indicates a good stability of the experimental apparatus.

The wavelength region of the the Hα line, which is contaminated by chromospheric emission in its core, and the spectral regions heavily affected by telluric lines (e.g. the $\lambda\,6276 - \lambda\,6315$ band of O_2), were excluded from the spectral band selected for the cross-correlation process of AR Lac spectra. Moreover the isolated telluric lines were interactively taken out by simple linear interpolation, both in the AR Lac and template spectra.

Fig. 1 show examples of CCFs at various orbital phases. The two peaks, more or less blended, correspond to each component of AR Lac. To better evaluate the centroids of the peaks (i.e. the radial velocity difference between target and template) we adopted two separate Gaussian fits for the cases of significant peak separation (i.e. near the quadratures), and a two-Gaussian fit algorithm to resolve cross-correlation peaks in blended situations.

An a-priori evaluation of the errors in the radial velocities of AR Lac is a difficult task due to the rotational broadening and flattening of the line profiles of both component. In addition, the profiles often display asymmetries and distortions arising from photospheric activity. This effect probably produces the double-peaked shape of the cool star CCF (see Fig. 1) implying a precision of the Gaussian fits lower than obtained from the narrower symmetrical CCF peaks of inactive stars. Presumably for these reasons AR Lac RV's display a scatter significantly larger than the 0.4 km s^{-1} limit deduced for standard stars.

Radial velocity values, listed in Table 1, are averages of the values obtained by the cross-correlation of each order of target spectra with the corresponding order of the standard star spectrum taken at the closest time. The standard deviation of the cross-correlation peak values of the different échelle orders has been adopted as an estimate of the errors on the radial velocity measurements. This error estimate is consistent with the dispersion of data points around the mean curve.

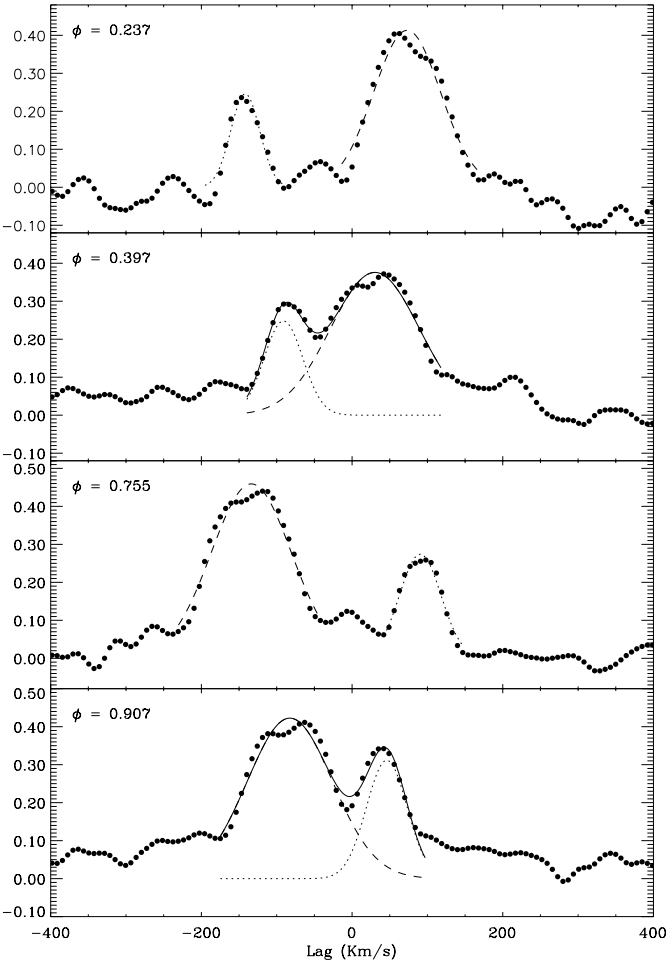

Fig. 1. Sample of Cross Correlation Functions (CCFs) between AR Lac and template spectra at different phases (dots). The Gaussian fits to the two peaks are displayed with a dashed line for the K0 IV component and with a dotted line for the G2 IV one. The full line represents the two-Gaussian fit for the blended cases.

Since AR Lac is well known to display period variations (e.g. Lanza et al. 1998), orbital phases have been reckoned from the following ephemeris: $\mathrm{HJD_{minI}} = 2447495.6369 + 1.983164 \times E$ (Pagano 1990) for 1994 and earlier data, and $\mathrm{HJD_{minI}} = 2450692.5174 + 1.983188 \times E$ (Marino et al. 1998) for 1996 and 1997 data.

The observational points and the associated errors are displayed in Fig. 2 as a function of orbital phase. The sinusoidal solution (full and dashed lines for the K0 and the G2 component respectively in Fig. 2), determined for a circular orbit, fits very well all the observations.

In Table 2 we report the orbital and physical parameters and related errors of AR Lac together with the last published orbital spectroscopic elements given by Sanford (1951), and revised by Popper (1980, 1990). The most evident difference with respect to Popper's (1990) solution and to the older ones by Harper (1933) and Sanford (1951) is given by the mass-ratio which is

Table 1. Radial velocities and equivalent widths of high resolution spectra.

HJD – 2440000	Phase	RV	$\sigma_{\rm RV}$	RV	$\sigma_{\rm RV}$	$W_{H\alpha}$(Å)	$\sigma_{\rm W}$	$W_{H\alpha}$(Å)	$\sigma_{\rm W}$	$W_{H\alpha}$(Å)	$\sigma_{\rm W}$
		K0 IV		G2 IV		K0 IV		G2 IV		K0 IV+G2 IV	
		(km s^{-1})								*blended*	
9618.5469	0.4663	1.1	±5.4	–	–					0.31	±0.05
9618.5615	0.4737	-4.8	2.0	–	–					0.38	0.04
9620.5764	0.4895	–	–	-29.4	±4.8					0.36	0.04
9620.5913	0.4971	–	–	-33.3	6.5					0.34	0.04
9621.5928	0.0022	-34.3	3.2	–	–	0.16	±0.06	–	–		
9621.6074	0.0096	-30.1	3.7	–	–	0.15	0.06	–	–		
9624.5566	0.4965	–	–	-27.9	0.7					0.31	0.03
9624.5715	0.5040	–	–	-32.4	2.1					0.29	0.03
9628.3662	0.4176	18.9	0.6	-98.3	2.1					0.22	0.04
9628.3809	0.4250	8.2	0.9	-97.2	5.1					0.21	0.04
9628.4199	0.4447	9.2	2.5	-72.9	16.1					0.19	0.03
9628.5529	0.5117									0.34	0.04
9628.6016	0.5362									0.34	0.05
9628.6168	0.5438									0.32	0.05
9630.4668	0.4768	-19.8	2.7	-42.5	8.3					0.30	0.05
9630.4824	0.4847	-22.5	1.3	-39.1	9.4					0.36	0.04
9643.4414	0.0192	-20.8	0.3			0.10	0.04	–	–		
10380.3389	0.5874	-88.0	11.6	29.5	4.3					0.30	0.12
10382.4902	0.6723	-129.3	4.2	74.0	2.1	0.34	0.08	0.08	±0.04		
10386.4189	0.6531	-125.4	2.7	63.2	3.9	0.25	0.02	0.08	0.02		
10388.4951	0.6999	-139.2	2.8	76.4	3.4	0.18	0.03	0.06	0.02		
10389.4580	0.1858	66.1	7.9	-143.4	4.5	0.35	0.04	0.14	0.03		
10390.4287	0.6750	-131.7	0.7	70.8	3.5	0.27	0.02	0.08	0.01		
10391.3789	0.1540	54.5	2.5	-132.7	3.1	0.14	0.02	0.06	0.01		
10392.3926	0.6652	-130.5	5.8	69.2	2.9	0.26	0.03	0.09	0.02		
10393.4834	0.2155	72.6	6.1	-154.2	4.1	0.11	0.03	0.12	0.02		
10394.3672	0.6611	-126.4	1.2	66.1	3.4	0.33	0.03	0.08	0.02		
10395.4971	0.2308	73.5	7.7	-154.6	1.5	0.26	0.03	0.12	0.02		
10406.3828	0.7196	-141.3	2.1	84.4	2.9	0.05	0.01	0.06	0.01		
10407.4131	0.2392	74.2	5.0	-154.0	2.8	0.32	0.02	0.09	0.01		
10638.5957	0.8105	-135.6	4.6	77.6	3.3	0.23	0.05	0.13	0.04		
10678.5527	0.9585	-56.9	3.0	–	–					-0.31	0.09
10680.4949	0.9378	-74.0	3.7	3.0	9.3					-0.48	0.06
10680.5996	0.9903	-40.2	0.4	–	–	-0.32	0.08	–	–		

significantly different from unity. The more evolved K0 IV star turns out to be a little more massive than the companion, consistent with a normal evolution of the two stars. It is interesting to note that the solution by Popper (1990) for the RV's of Ca II emission lines is closer to our solution than that he obtained from the photospheric absorption lines. This may be due to the severe blending of lines from the two components in the blue-violet region covered by the Sanford's (1951) spectrograms.

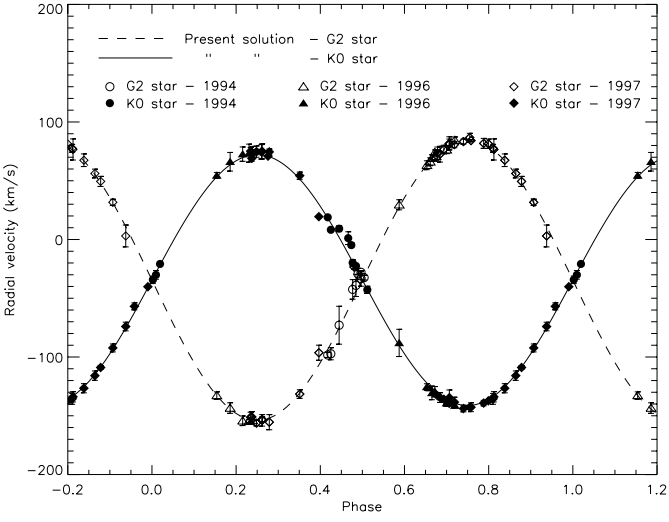

Fig. 2. Radial velocity curve and best-fit solution of AR Lac

4. Extraction of Hα emission

It is well known that the Hα line does not provide "direct" information on chromospheric main parameters (temperature and density of the line forming layer) like optically thin CD lines lines do, but it contains valuable information on the chromospheric structure (Cram & Mullan 1985). However, it has been shown, on empirical grounds (correlations with other chromospheric diagnostics and X-ray flux) that one can derive reason-

Table 1. (continued)

HJD – 2440000	Phase	RV K0 IV	$\sigma_{\rm RV}$	RV G2 IV	$\sigma_{\rm RV}$	$W_{\rm H\alpha}$(Å) K0 IV	$\sigma_{\rm W}$	$W_{\rm H\alpha}$(Å) G2 IV	$\sigma_{\rm W}$	$W_{\rm H\alpha}$(Å) K0 IV+G2 IV *blended*	$\sigma_{\rm W}$
		(km s^{-1})									
10681.5708	0.4803	–	–	-23.4	1.7					0.41	±0.07
10752.4785	0.2345	75.2	3.1	-151.2	4.3	0.17	±0.07	0.05	±0.07		
10754.3808	0.1939					0.14	0.05	0.11	0.04		
10754.4668	0.2372	69.1	2.5	-151.0	4.6	0.15	0.04	0.07	0.02		
10755.3418	0.6784	-132.9	0.6	73.5	5.2	0.40	0.10	0.07	0.04		
10756.3634	0.1936					0.15	0.08	0.12	0.06		
10758.4824	0.2618	75.1	6.5	-153.9	4.9	0.19	0.06	0.09	0.04		
10758.5098	0.2758	70.9	0.7	-153.0	2.2	0.23	0.06	0.09	0.03		
10759.2861	0.6674					0.08	0.06	0.04	0.03		
10759.3379	0.6935	-135.9	2.3	76.6	3.6	0.14	0.07	0.06	0.03		
10759.3877	0.7186	-138.4	4.2	80.7	2.7	0.13	0.03	0.07	0.03		
10759.4307	0.7401	-143.8	2.8	83.3	2.1	0.13	0.04	0.07	0.04		
10759.4658	0.7580	-142.7	3.8	84.1	0.9	0.13	0.03	0.07	0.02		
10763.4268	0.7551	-142.8	1.9	86.7	3.7	0.20	0.04	0.07	0.02		
10763.4922	0.7881	-139.2	2.3	81.8	4.2	0.26	0.07	0.10	0.03		
10763.5146	0.7993	-137.3	1.1	81.4	4.0	0.18	0.05	0.06	0.04		
10764.4053	0.2484	74.8	4.8	-157.0	1.2	0.25	0.06	0.14	0.03		
10764.4287	0.2604	74.6	6.2	-156.2	2.4	0.24	0.06	0.13	0.04		
10765.2695	0.6845	-134.5	4.1	72.6	6.7	0.12	0.06	0.05	0.03		
10765.3135	0.7066	-134.6	6.6	81.1	4.3	0.20	0.09	0.10	0.05		
10768.4316	0.2788	74.5	2.5	-155.4	6.4	0.26	0.03	0.11	0.03		
10769.2793	0.7063	-139.4	2.2	81.6	5.7	0.25	0.06	0.06	0.03		
10797.3057	0.8383	-126.6	3.9	67.4	5.4	0.23	0.03	0.02	0.02		
10801.2207	0.8124	-133.9	4.4	76.6	9.0	0.37	0.07	0.06	0.03		
10803.3076	0.8645	-115.8	4.0	56.1	3.7	0.20	0.03	0.00	0.00		
10804.2725	0.3511	54.3	3.1	-131.5	3.7	0.39	0.03	0.11	0.02		
10805.3174	0.8781	-108.9	1.7	49.4	4.3	0.18	0.03	-0.01	0.01		
10811.3242	0.9070	-92.3	3.4	31.6	2.7	0.08	0.03	-0.08	0.03		
10812.2959	0.3967	19.4	0.6	-96.3	6.4	0.15	0.03	0.07	0.02		

Table 2. Orbital elements of AR Lacertae

	Present solution	Popper (1990) absorption	Popper (1990) emission
K_h (km s^{-1})	119.43 ±0.49	116.5	117.4
K_c (km s^{-1})	106.73 ±0.29	113.1	106.7
γ (km s^{-1})	-34.54 ±0.5		
γ_h (km s^{-1})		-34.6	-38.5
γ_c (km s^{-1})		-31.7	-37.6
e	0	0	0
$a_h \sin i$ (10^6km)	3.257 ±0.013	3.2	3.1
$a_c \sin i$ (10^6km)	2.911 ±0.008	3.1	2.9
$m_h \sin^3 i$ (M$_\odot$)	1.122 ±0.008	1.22	1.06
$m_c \sin^3 i$ (M$_\odot$)	1.255 ±0.011	1.26	1.12
m_h/m_c	0.894 ±0.006	0.97	0.94

Note: h: hotter, c: cooler

able estimates of the chromospheric emission at Hα by subtracting out the underlying photospheric absorption spectrum (Herbig 1985, Barden 1985, Strassmeier et al. 1990, Pasquini & Pallavicini 1991, Frasca & Catalano 1994). The comparison of the observed spectrum with a synthetic one is of fundamental importance for the analysis of the emission, in double-lined system. In fact, disentanglement of the composite profile is nearly impossible in their complex spectra, where lines are generally rotationally broadened and show variable blending due to the radial velocity shifts.

To simulate the inactive spectrum of AR Lac we observed, as reference stars, two slow-rotating inactive stars of the same spectral type as the AR Lac components, namely 51 Peg (G2 V-IV) and δ Eri (K0 IV). We have taken several exposures of our standard stars and have chosen for each season the highest S/N spectra as template. In order to reproduce the exact shape of the photospheric Hα profile, the spectrum of each reference star normalised to the continuum was convolved with the rotational profiles of $v \sin i = 38$ km s^{-1} for the G2 component and $v \sin i = 68$ km s^{-1} for the K0 one. A linear limb-darkening coefficient $\mu = 0.65$ and $\mu = 0.70$ (Al-Naimiy 1978) has been adopted for the hotter and cooler component respectively. The $v \sin i$ values have been directly derived from the orbital solution assuming co-rotation for both components through the relation

$$v \sin i_{\rm h,c} = \frac{2\pi}{P} R_{\rm h,c} \sin i \qquad (1)$$

where the inclination $i = 87°$ and the relative radii $r_{\rm h,c}$ are derived from the photometric solution by Lanza et al. (1998), and the absolute radii, $R_{\rm h,c}$, are computed from the binary separation ($a = 6.176 \times 10^6$ km) resulting from our RV solution.

The synthesised spectra, broadened with these $v \sin i$ values, reproduce very well the AR Lac spectra. Telluric lines were not taken out, in the reference spectra and they are washed out by the rotational broadening procedure. Since they were not taken out also in the AR Lac spectra they appear as small absorption features, of instrumental width in the difference spectra (Fig. 4). From the Moore et al.'s catalogue (Moore et al. 1966) we can see that the $\lambda 6564.206$ Å is the only important telluric feature blended with the Hα line. Its listed equivalent width is 14 mÅ which is much smaller than the equivalent width of the measured Hα excess emission, i.e. its contribution is well within the estimated error of the emission evaluation. The position of that and other relevant telluric lines is indicated in Fig. 4.

The treatment of the rotationally broadened line-profile is very complex when the system is in a partial-eclipse configuration (phase near to 0 or 0.5). In these cases the reference spectra cannot be simply convolved with a normal rotational profile because the portion of the occulted stellar disk does not contribute to the observed line profile. Therefore we have computed the "eclipse-rotational" profiles by considering the visible area, velocity shift, and limb-darkening for each strip of the occulted stellar disk parallel to its rotational axis. Two configurations of eclipse-rotational profiles are displayed in the insets of Fig. 3, which shows the Hα spectra of the reference stars broadened with these distorted profiles and compared with the non-distorted ones (dotted lines). The consequences of the eclipses are a variable broadening, deformation and also shifts of line profiles.

After convolution with the appropriate rotational profile, we added the two reference spectra, properly weighted and Doppler-shifted according to RV solution derived in Sect. 3. The contributions of the two stars to the combined spectrum at the Hα wavelength have been evaluated from radii and effective temperatures as 0.34 and 0.66 for the hot and cool component, respectively. During the eclipses these weights have been properly corrected taking into account the light contribution of each star at each phase. The wavelength alignment of the synthetic and AR Lac observed spectra has been improved by cross-correlation. To define the net Hα emission of the two components we have subtracted the synthetic spectrum from each AR Lac spectrum. In the difference spectrum the absorption lines cancel out and the excess emission of the two components in the Hα core appears as a positive residual well above the noise (Fig. 4). The net equivalent width (EW) of the Hα emission has been evaluated on the difference spectra integrating along the residual emission profile (separately for each components whenever these were easily isolated, elsewhere a cumulative integration has been performed). The errors on the measured EW were estimated determining the S/N in two windows on the right and left-hand side of Hα in the difference spectrum. In Fig. 4a sample of spectra analysed with such procedure is shown.

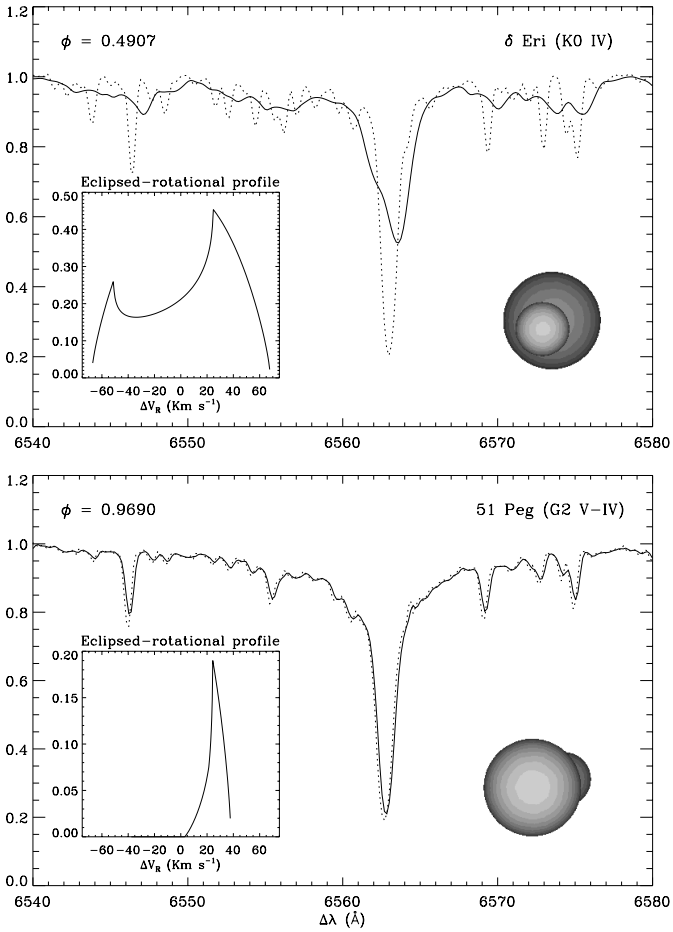

Fig. 3. Simulation through standard star spectra of the effect of eclipses at transit (upper panel) and occultation (lower panel) on the photospheric lines of the occulted stars. The distortion (upper panel) and wavelength shift (lower panel) that results from the convolution of the standard star spectrum with the eclipse-rotational profile (solid line) is made evident by the comparison with the observed one (dotted line). The eclipse-rotational profiles (insets) and the system configuration at each phase are also shown.

The first outstanding result of this analysis is the presence of appreciable net Hα emission from both components in most of the observations. This result is similar to what observed by Liu & Tan (1986), Frasca & Catalano (1994) and Montes et al. (1995).

Net EW measurements are listed in Table 1 together with the estimated errors.

5. Results

5.1. Hα equivalent width

In the following we analyse the excess emission of both components separately, at the phases in which the net Hα profiles are easily isolated, and the total integrated emission for the blended configurations.

Let us first discuss the data obtained at low resolution, e.g. those of 1989 and 1990 (Table 3).

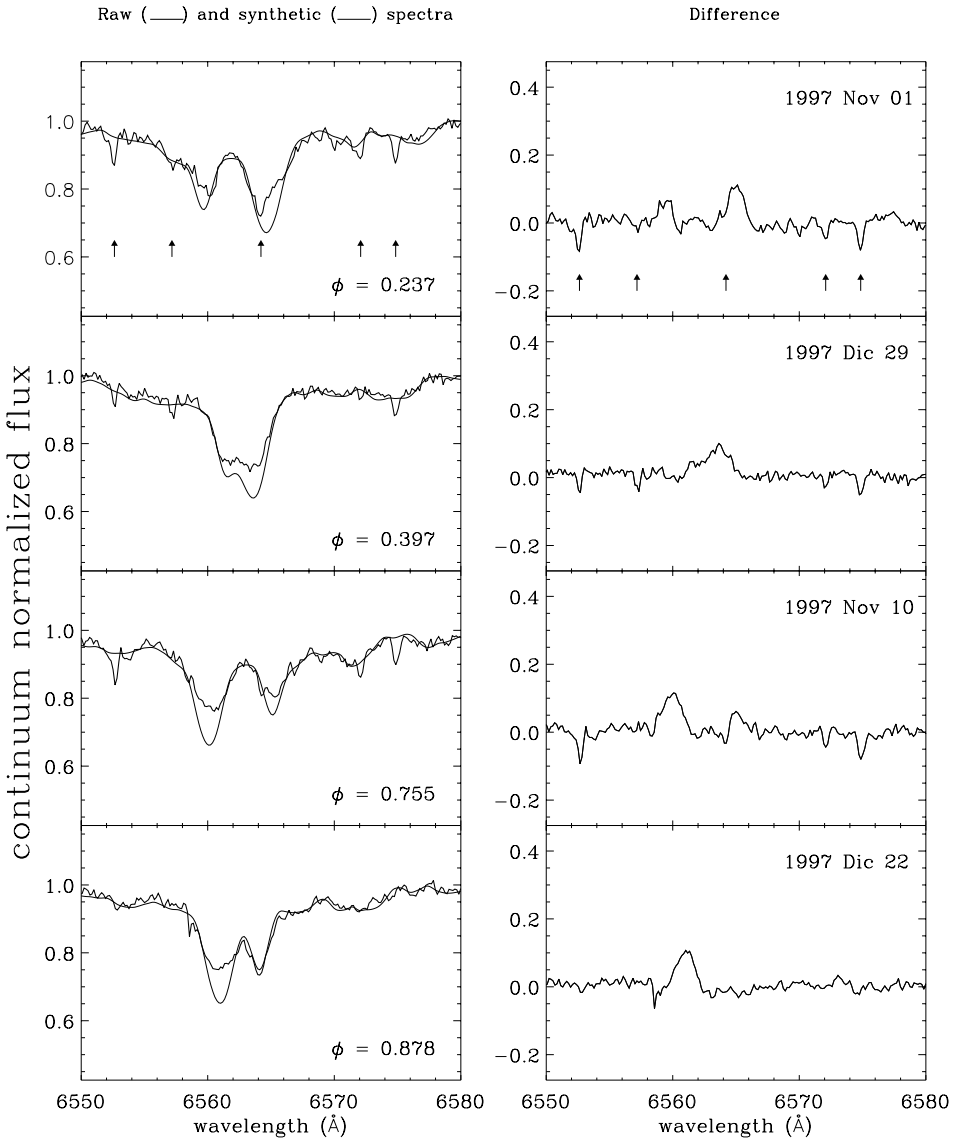

Fig. 4. *Left*: Sample of observed spectra of AR Lac (*thick lines*) at different orbital phases with superimposed the synthesised inactive spectra (*thin lines*). *Right*: The difference spectra which show Hα emission from both the system's components. Vertical arrows mark the telluric lines present in this spectral region.

Fig. 5 shows the time variations of Hα emission for each component in 1989. The most striking feature is the presence of high values of the Hα EW's at JD=2447798 and 2447799 for the cool component only. They indicate the occurrence of a flare on the K0 IV component as it is discussed in Sect. 6.3. The emission arising from the G2 V component seems to remain more or less constant.

The 1990 data of the cool star show a nearly constant trend, with EW values between 0.15 and 0.3 Å, i.e. the same quiescent level observed in 1989. A small difference between the 1^{st} quadrature points, slightly higher than those near to $\phi = 0.75$, is found in 1989 and 1990 EW's of the G2 component.

The spectra obtained since 1994 were acquired in the cross dispersion mode, which, due to the higher resolution, has allowed us to separate the emission of the two components even close to the eclipses and therefore to better define possible changes with the orbital phase.

In Fig. 6 the EW's obtained from high resolution spectra in 1994, 1996 and 1997 are plotted separately for the two components. An important result of the comparison is the larger scatter of the excess emission of the K0 IV component $\sim 40\%$, i.e. more than twice the estimated average errors in the measurements, with respect to that of the G2 IV one. The spread in the measurements of the latter star is consistent with the average measurement errors, thus indicating a greater instability of the cooler star chromosphere. This result is in agreement with Hall & Wolowitz (1998) analysis who found a total variability for the Hα excess emission of 58.9% and 27.1% for the K0 IV and G2 IV, respectively. We wonder how much of the spread we observed in Hα emission of the cool star could be the result of many unresolved small flares as clearly detected at X-ray wavelength from Beppo-SAX observations (Rodonò et al. 1999).

The average EW emission values of the K0 component (0.15–0.30 Å) are slightly larger than those of the G2 (0.05–0.15), and are similar to that observed in 1989 and 1990, for each

Table 3. Hα equivalent widths from low resolution spectra.

HJD – 2440000	Phase	$W_{H\alpha}$(Å) K0 IV	$W_{H\alpha}$(Å) G2 IV	$W_{H\alpha}$(Å) K0 IV+G2 IV
7794.471	0.692	0.19 ± 0.04	0.16 ± 0.05	0.35
7794.617	0.766	0.18 ± 0.04	0.15 ± 0.05	0.32
7795.406	0.164	0.21 ± 0.03	0.18 ± 0.04	0.39
7795.560	0.241	0.24 ± 0.04	0.18 ± 0.05	0.42
7795.579	0.251	0.27 ± 0.04	0.20 ± 0.05	0.48
7796.516	0.723	0.16 ± 0.04	0.07 ± 0.04	0.23
7796.616	0.774	0.18 ± 0.04	0.12 ± 0.04	0.30
7797.396	0.167	0.12 ± 0.03	0.18 ± 0.04	0.30
7798.446	0.696	0.41 ± 0.05	0.16 ± 0.04	0.57
7798.621	0.785	0.50 ± 0.05	0.03 ± 0.04	0.53
7799.444	0.200	0.31 ± 0.04	0.19 ± 0.04	0.50
7799.599	0.278	0.25 ± 0.04	0.21 ± 0.05	0.46
7800.502	0.733	0.10 ± 0.03	0.14 ± 0.04	0.24
8107.595	0.576	–	–	0.19
8107.598	0.578	–	–	0.21
8109.597	0.586	–	–	0.26
8109.601	0.588	–	–	0.28
8111.590	0.591	0.14 ± 0.03	0.04 ± 0.02	0.18
8111.594	0.593	0.14 ± 0.03	0.05 ± 0.02	0.19
8132.615	0.193	0.19 ± 0.06	0.08 ± 0.03	0.27
8133.622	0.701	0.23 ± 0.03	0.12 ± 0.04	0.35
8135.592	0.694	0.24 ± 0.04	0.14 ± 0.04	0.38
8136.590	0.197	0.18 ± 0.04	0.01 ± 0.05	0.19

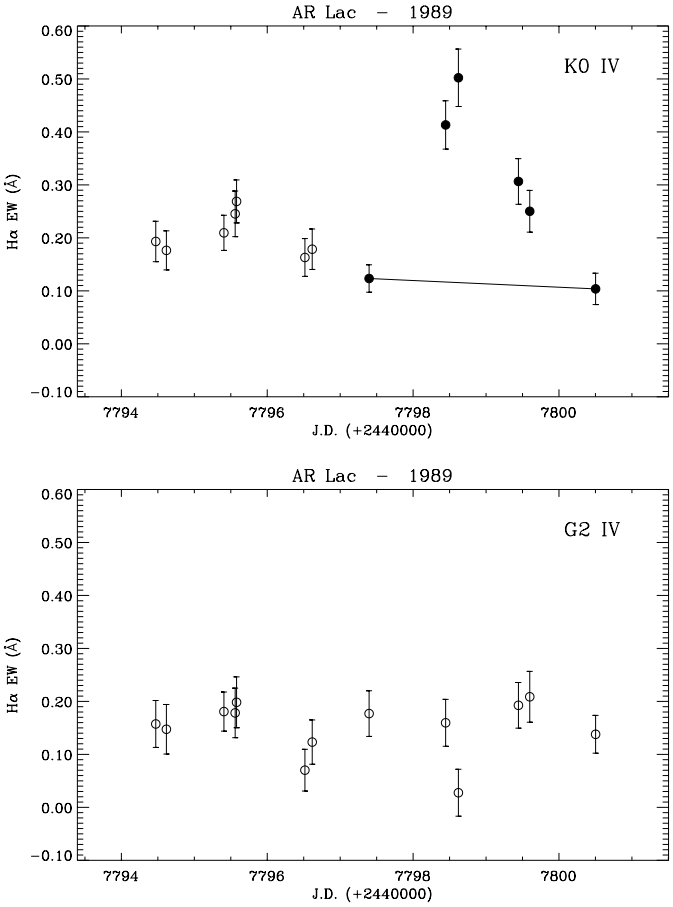

Fig. 5. Equivalent width of Hα emission from the individual components of AR Lac vs time for low resolution data (1989). The flare eruption on the K0 component (filled symbols in the upper panel) is obvious.

component, respectively. This suggests that the excess emission extraction through the spectrum synthesis method works comparably well at low and high dispersion, and, that no significant changes have occurred in the chromospheres of both components along the time span of our observations.

Montes et al. (1997) in 1995 measured a net emission EW outside eclipses of 0.169 and 0.248 Å for the G2 and K0 components, in very good agreement with our average values. Huenemoerder & Ramsey (1984) did not separate the excess emission of the two components and gave a plot of the cumulative net Hα emission which have an average value of about 0.2 Å, i.e. about half of our and Montes et al. (1997) values when the emission of both components are summed up.

To compare our results with Bopp & Talcott (1980) observations, we estimated the absorption equivalent width at various orbital phases. As done by Bopp & Talcott the measured EW is the sum of the two resolved stellar lines. By considering a sample of spectra acquired outside eclipse, we obtain an average total EW of Hα absorption line of -1.69 $\pm$ 0.09 Å, which within 10% agrees with the average value of -1.54 Å found by Bopp & Talcott (1980).

No clear rotational modulation is evident in the EW emission curve of both components, apart from a slight asymmetry in the maxima of the G2 component which is a little brighter at first quadrature, i.e. the leading hemisphere appears brighter than the trailing one as we found in 1989–1990, and as very often found in the Mg II observations, but in the opposite sense (Neff et al. 1989, Neff 1992, Pagano et al. 1994). The brightening in the Mg II is seen in both stars on the trailing hemisphere and reaches about 50%. The effect in the Hα is seen only in the G2 IV component with a brightening of the leading hemisphere that leads to an EW variation of about 30%. The spread of the data does not allow us to define any significant difference in the Hα emission between the two hemispheres of the K0 IV component; the average EW emission being ~ 0.22 Å for both hemispheres.

Asymmetries in the Ca II emission were already noticed by Sanford (1951), who found an emission EW of the H and K line larger at the first quadrature (phases 0.15–0.35) than at the second one (phases 0.6–0.9). However, the emission ratio seems to increase progressively in the first half-period and decrease in the second half-period. Sanford called also attention to changes in the depth of photospheric absorption lines of the G2 star (Fe I $\lambda\lambda$ 4045, 4063, and 4071). The lines of this star have the relatively strongest absorption at the second quadrature when the G2 star is receding faster, i.e. when the trailing hemisphere is facing the observer. The phenomenon can be easily interpreted in terms of absorption material in front of the trailing hemisphere of the G2 component, as clearly shown by the extra absorption we observed in the Hα profile in 1997, which will be discussed in Sect. 6.1.

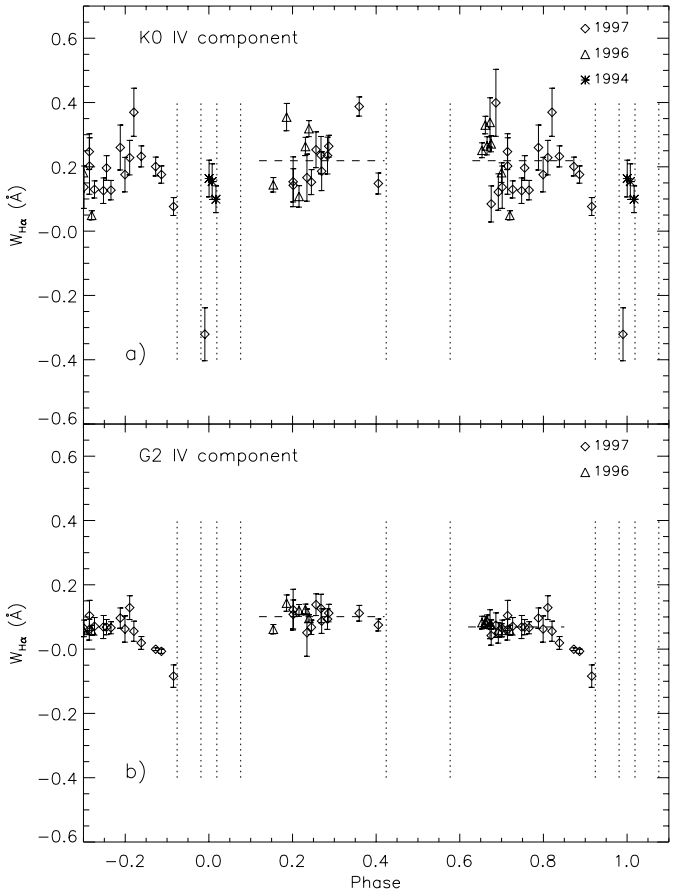

Fig. 6a and b. Hα equivalent width of the individual components of AR Lac plotted against orbital phase for high resolution data. The *vertical dotted lines* mark the phase of eclipse's contacts. The *horizontal dashed lines* represent the mean levels outside eclipse. Different symbols refer to different season of observations.

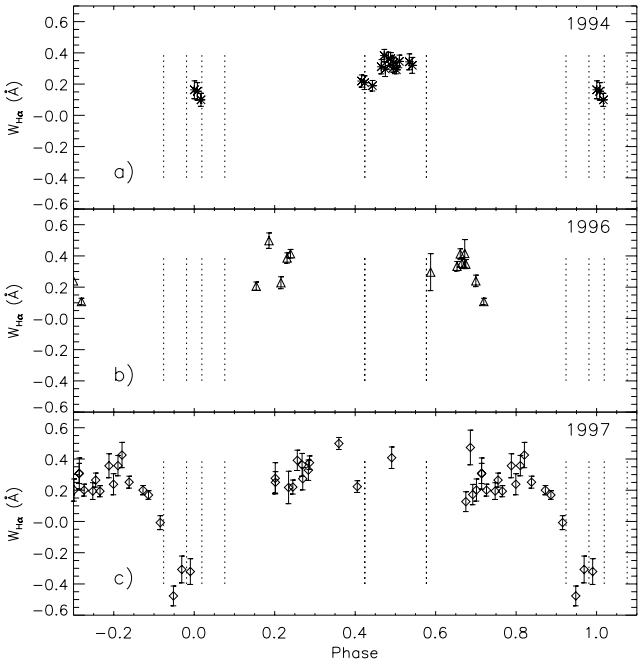

Fig. 7a–c. Equivalent width of Hα total emission of AR Lac plotted versus the orbital phase for the high resolution data.

A clear decrease of emission in both components is seen before the primary eclipse in 1997 and the net Hα profile goes to absorption in the spectra near the totality (Fig. 6).

To better analyse this issue, we have considered the "total" Hα EW in the difference spectra, i.e. the emission integrated all over the profile thus producing a coherent picture also at phases in which the strong blending prevents us from distinguishing the contribution from each component. In Fig. 7, where the "total" EW's are separately plotted for the three high resolution observing runs, we see that the 1997 data present a striking decrease in net Hα EW, which goes from emission to absorption approaching the primary eclipse. Data acquired between the first and the second contact of primary eclipse, when both components are visible and are too blended for decoupling their contributions, indicate that both stars are affected by absorption (Figs. 6 and 7). We would like also to emphasise that the three data points inside the primary eclipse were obtained two days apart, but the point just before the first contact (phase 0.907), that substantially confirms the extra-absorption, refers to a spectrum taken about 130 days later, thus indicating a feature lasting at least 65 orbital cycles.

However, the excess absorption during the primary eclipse, clearly evident in 1997, is not observed in 1994, when the emission level was comparable with that outside eclipse (Fig. 7).

Such a steep decrease in Hα EW near the primary eclipse could be explained by the occultation of an emitting region located between the two components, but the inspection of observed and synthesized spectra allows us to envisage an extra-absorption rather than a simple decrease of emission, as we will discuss in the next chapter.

5.2. Radial velocity of the Hα emission

The Hα absorption profile is often asymmetrically filled-in, thus giving rise to a radial velocity of the net emission, which is different from that of the photospheric absorption lines. The radial velocities of the Hα emission cores can therefore give additional constraints to the location of the chromospheric inhomogeneities.

The determination of radial velocities of Hα emission was performed, for high-resolution data only, by measuring the central wavelength of the residual emission in the difference spectra and by correcting for the Earth motion. The position of emission wavelength centroid was determined, for each component of AR Lac, from Gaussian fits to the data obtained near quadratures or during total eclipse. Spectra acquired in orbital configurations corresponding to blended Hα emission lines were not considered.

Fig. 8a shows the radial velocities of the net Hα emission with the superimposed sinusoidal photospheric solution[2]. In

[2] We recall that the photospheric radial velocities (Sect. 3) were determined excluding the Hα line

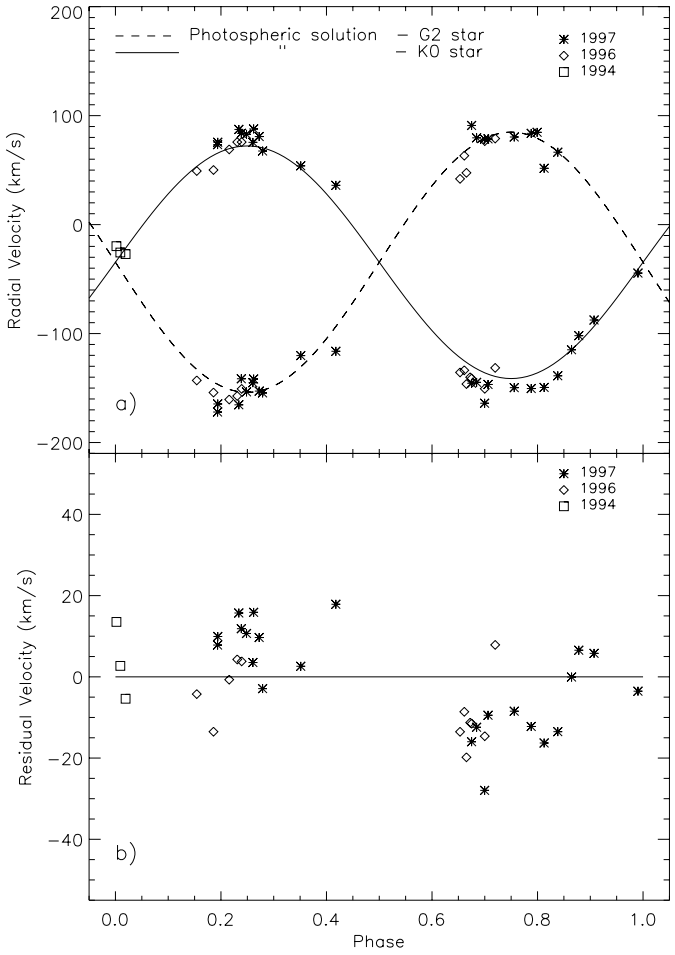

Fig. 8. a Radial velocities of the net Hα emission. Continuous curve and dashed curve represent our photospheric solution for the cooler and hotter component, respectively. **b** Difference between chromospheric and photospheric radial velocities for the cool component of AR Lac

spite of the scatter of the values, the chromospheric radial velocities of the K0 star appear to have a larger amplitude than the photospheric curve, especially close to the quadratures. The G2's chromospheric radial velocities very closely follow the photospheric solution, thus indicating a uniform distribution of emission on the stellar surface.

The difference between chromospheric radial velocities of the K0 star and the photospheric solution is plotted in Fig. 8b where a velocity excess $\Delta V_{\rm r} \simeq 10$ km s^{-1} is clearly visible. This velocity excess of the K0 IV star Hα emission is in the opposite sense of the average velocity difference observed for the Mg II emission (Neff et al. 1989). The large discrepancy of about 25 km s^{-1} they initially found at $\phi = 0.75$ was partly accounted for, by adding to the fit another discrete emission component on the red wing of the K star emission profile. The Mg II radial velocity of the K0 star, after allowing for all discrete emission components due to isolated plages, is completely consistent with our new orbital solution.

To explain this Hα emission velocity excess we may either suppose the presence of chromospheric active regions evenly distributed, with some enhancement in the hemisphere of the cool star far from the companion, or simply consider the gravity darkening effect, on the distorted cool star. The average difference of radial velocity can then be converted into a distance of emission photocenter from the star center. From an average $\Delta V_{\rm R} \approx 10$ Km s^{-1} at the quadratures, a distance of about 0.15 $R_{\rm cool}$ of the emission photocenter from the K0 IV rotation axis can be estimated.

6. Discussion

6.1. Primary eclipses

The most outstanding feature in Fig. 7c is the presence of excess absorption at primary eclipses in 1997, preceded by a decrease in the emission just before the 1$^{\rm st}$ contact.

The behaviour of the phenomenon is better described by the analysis of the difference spectra shown in Fig. 9 together with the configuration of the system.

The spectra at phases $0^{\rm P}.864$ and $0^{\rm P}.878$ show clear indication of excess absorption at the wavelength of the G2 star whose Hα line becomes as deep as that of the K0 star (see the lowest panel in Fig. 4). Normally the depth ratio is about 0.8. Furthermore, at these phases the effect is revealed by: a) a decrease in the net Hα EW, b) the disappearance of emission in the Hα core of the G2 star, c) a flattening of the residual emission coming from the cool component. However, the most important absorption effect on the Hα emission begins between 0.878 and 0.907 phases, when we observe a clear absorption feature at the spectral position of the G2 (Fig. 9). As the eclipse proceeds the emission of the cool star disappears ($\phi = 0.938$) and the absorption shifts to the red at about 40 km s^{-1} from the hot star centre which corresponds to the velocity of its receding visible edge.

The extra absorption is also seen during totality, when only the spectrum of the cool K0 component is visible. During the totality ($\phi = 0.990$), the absorption extends in the blue side producing an asymmetrical emission of the cool star and has a center position shifted to the red by 68 km s^{-1} (i.e. equal to the v$\sin i$ of the K0 star), consistent with an absorption affecting the receding edge of the visible star.

The lowest panel of Fig. 9 shows the spectrum taken at totality in 1994, where a weak emission from the K0 star but no absorption is visible indicating that the phenomenon was not present at that time. Although we did not find evidence of extra absorption in 1994, the phenomenon was observed in the past. It is clearly visible in the spectra of Nations & Ramsey (1980) taken on September 1979 when the Hα depth of the G2 star increased by about the 60% at phases 0.771, 0.806 and 0.822 becoming deeper than that of the K0 star. A marginal evidence of extra-absorption can be found also in the difference spectra of Huenemoerder & Ramsey (1984) taken at phase 0.91 and 0.96 in 1982, September 29 and October 5. Finally, Montes et al. (1997) detected an excess Hα absorption at orbital phase $0^{\rm P}.939$, at the wavelength position of the hot component.

The lack of observations at the egress of primary eclipse prevents us from establishing whether the distribution of the

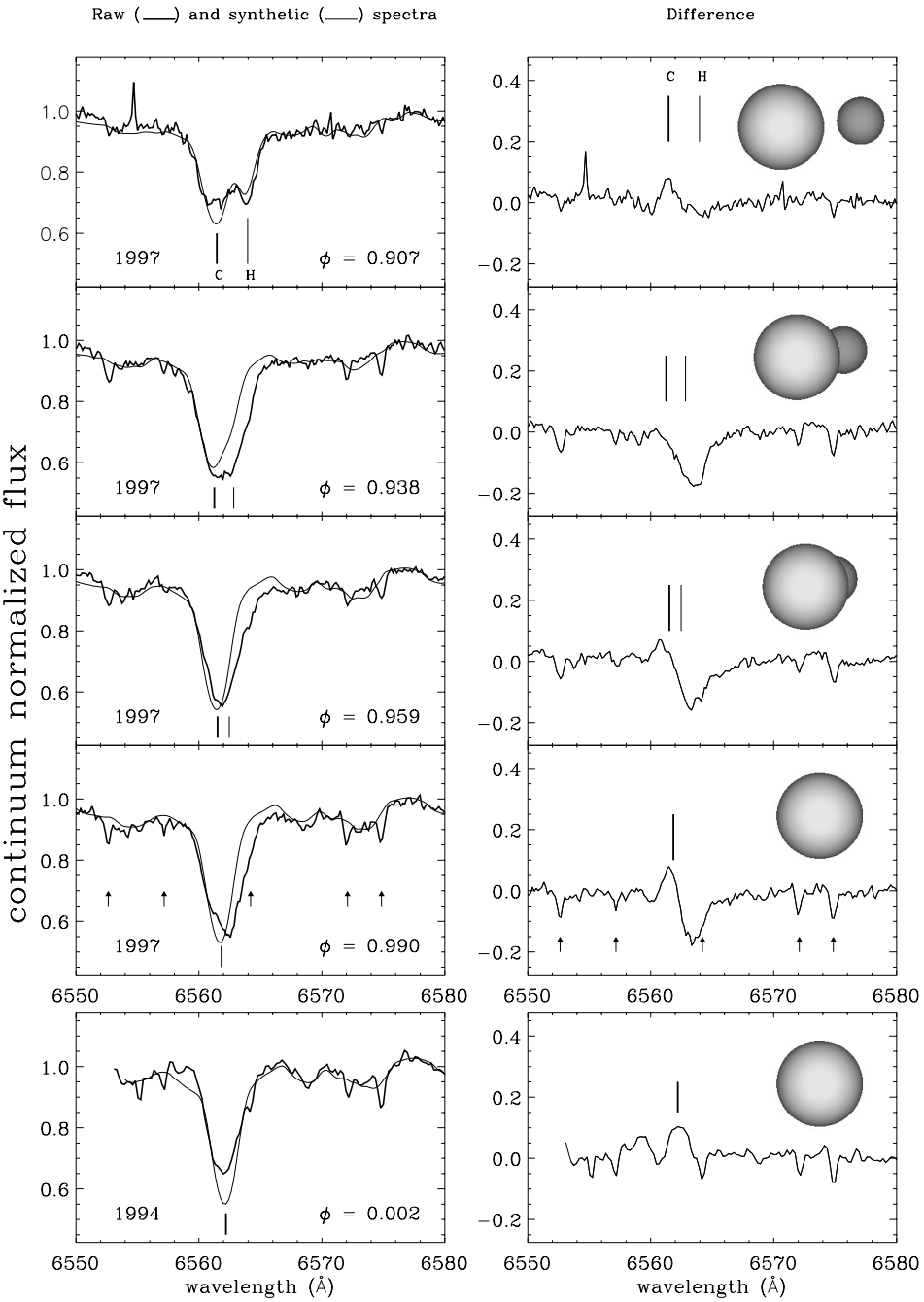

Fig. 9. Sequence of spectra taken in 1997 near the primary eclipse showing absorption excess. The observed spectra (thick lines) and the synthesized one (thin lines) are shown on the left side. The difference spectra are displayed on the right side together with the pictures of the configuration of the system. In the lower panel a 1994 spectrum at totality is also shown. Vertical arrows mark the telluric lines present in this spectral range.

absorbing material around the cool star is spherically symmetric or not. Therefore, the hypothesis already proposed by Montes et al. (1997), to explain their spectrum of AR Lac at phase 0.939 of a prominence-like absorbing structure extended off the limb of the cool component seems to apply also to the interpretation of our data. On the other hand, the presence of absorption on the K0 star during the totality seems to rule out the case of mass transfer from the K0 toward the G2 star that normally is expected to take place at L_1 point which is not visible during the eclipse.

Excess absorption or deficiency of emission from the G2 star at the egress from primary eclipse was seen in different chromospheric and coronal diagnostics in various occasions: e.g. the EXOSAT LE light curve (White et al. 1990), the ASCA light curve (White et al. 1994), and the integrated Mg II light curve (Neff et al. 1989). A similar asymmetric light curve was found during the second of the two orbits of continuous monitoring with EUVE performed by Walter (1996). Among others, he suggested the geometrical occultation by optically thick material as the most likely explanation. He estimated that the cool, dense material should be confined within 15° of the equator of the K0 star and extend outward by $\sim R_{\rm K0}$; the inferred density $n_{\rm e}$ was in the range 10^{11}-$10^{12}\,cm^{-3}$, i.e. similar to solar-prominence density.

To estimate the main properties of the material causing the extra Hα absorption, we propose a simple model to fit the Hα line during the totality, when only the K0 IV star is visible, i.e. the easiest configuration to analyse.

In the framework of the solar-prominence analogy, we make the hypothesis that the absorbing material (a slab of uniform density and thickness L) has negligible intrinsic emissivity and is located above the receding edge of the K0 star surface.

Furthermore, we assume that the occulted part of the stellar disk is simply delimited by an inclined chord. Under these assumptions, each strip of the star disk will undergo a different absorption depending on the fraction of its light that is intercepted by the slab. The observed Hα profile will be at each wavelength the sum of the absorbed and non-absorbed contributions of each strip. Therefore, we can write the surface flux (normalized to the local continuum F_c) as

$$\frac{F_\lambda}{F_c} = \sum_{i=1}^{n} \frac{I^0_\lambda(\lambda - \Delta\lambda_i)}{I_c} \left(a_i + b_i e^{-\tau_{\lambda-\Delta\lambda_i}}\right) \quad (2)$$

where $\Delta\lambda_i$ is the wavelength shift of the $i^{\rm th}$ strip, $\frac{I^0_\lambda}{I_c}$ is the normalized intensity-spectrum that we assume independent of the position over the stellar disk, a_i and b_i are the light contributions of the non-absorbed and absorbed part of the $i^{\rm th}$ strip, respectively, and $\tau_\lambda = \int_0^L \alpha_\lambda N_2 d\ell \simeq \alpha_\lambda N_2 L$ is the slab's optical depth. We have denoted with α_λ the atomic absorption coefficient and with N_2 the number of absorbers per cm^3 in the lower level ($n = 2$) of the Hα transition.

The density number N_2 has been evaluated in typical solar prominences conditions (temperature $T \sim$ 6000–8000 K and electron density $n_{\rm e} \sim 10^{11} - 10^{12}\, cm^{-3}$, on the average) using the diluted Boltzmann equation (dilution factor 1/2 near the star surface) and Saha ionization equation. In such physical conditions, the thermal broadening of the Hα line dominates over all other broadening effects, like collisional damping and linear Stark effect (see eg. Griem 1962, Gray 1992). So, the atomic absorption coefficient is

$$\alpha_\lambda d\lambda = \frac{\pi^{1/2} e^2}{mc} f_{2-3} \frac{1}{\Delta\lambda_{\rm D}} \exp\left[-(\frac{\Delta\lambda}{\Delta\lambda_{\rm D}})^2\right] d\lambda \quad (3)$$

where $f_{2-3} = 0.6407$ is the oscillator strength of the Hα transition, $\Delta\lambda_{\rm D} = \frac{\lambda_0}{c}\left(\frac{2kT}{M} + \xi^2\right)^{1/2}$ is the Doppler-width of the line and ξ is the micro-turbulence velocity.

The residual profile of Fig. 9 at phase 0.99 has been fitted by means of a trial-and-error procedure in which we let the slab's thickness L, the electron density $n_{\rm e}$ and the obscured portion of the stellar disk to vary. The slab temperature was fixed to 7000 K. We assumed a uniform chromospheric emission of the K0 star, yielding a Gaussian emission profile, reproduced by fitting the difference spectra at second quadrature, when they are not affected by extra absorption. We found a good fit of the observed extra-absorption with $n_{\rm e} = 6 \times 10^{11}\,{\rm cm}^{-3}$, $L = 3 \times 10^5$ km and an obscured fraction of 40% of the star disk. The fit improved if a red-shift of about 25 km s^{-1} and a micro-turbulence velocity $\xi = 14\,{\rm km\,s}^{-1}$ for the slab were considered.

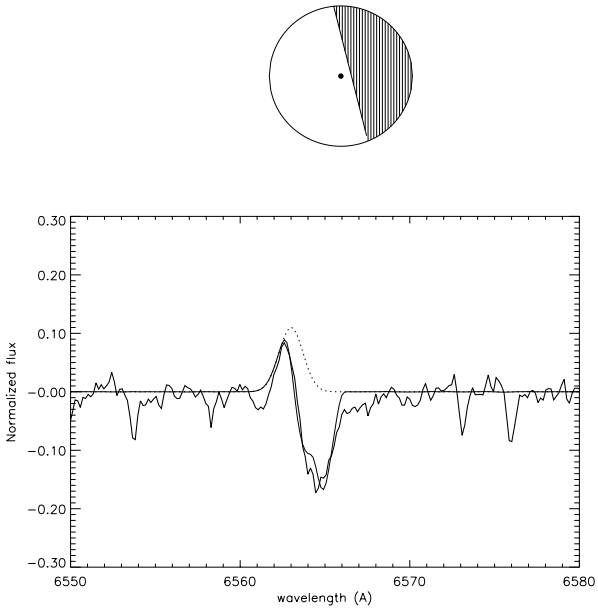

Fig. 10. Fitting of the extra absorption spectrum seen during the totality phase in 1997. The observed residual spectrum is displayed with a thick line, while the Gaussian in dotted line simulates the core emission. The fit of the extra-absorption is displayed with a thin line. In the upper panel a schematic drawing of the star disk is shown with the occulted part hatched.

The profile fit is shown in Fig. 10 together with a schematic drawing of the star disk with the obscured part indicated by the hatched region.

Solar prominences have typical thickness of 1–5$\times 10^4\, km$ and electron densities of $10^{11} - 10^{12}\, cm^{-3}$. The value of density we found for AR Lac is consistent with the solar one, while the thickness results to be about one order of magnitude larger.

The absorption effects on the G2 star begin about at phase 0.85, therefore this prominence-like structure should be anchored on the leading hemisphere of the cool star and extends up to 3 R$_\odot$ (projected separation of the two star limbs). Since the velocity of the absorption feature is consistent with the velocity of the absorbed star, or star limb, the absorbing material could be assimilated to a static or quasi-static loop, with plasma overall velocities no more than 20–30 km s^{-1}. Similar structures have been first proposed for the eclipsing binary V471 Tau (K2 V + DA2) by Guinan et al. (1986) and more recently for the RS CVn system SS Boo by Hall et al. (1990). In a dedicated survey of the phenomenon Hall & Ramsey (1992) found extended material in eight of the ten monitored RS CVn systems. Although they found cases where two loops could be present, the most frequent situation is that of a loop on the leading hemisphere of the cool star as we found in the case of AR Lac.

Although the comparison of our 1994 and 1997 data does indicate a transient phenomenon, the past observations do suggest a more permanent configuration, probably connected with the sector structure of active longitudes around the sub-stellar point of the cool component detected from the analysis of long-term photometry (Lanza et al. 1998).

6.2. Secondary eclipses

As seen in Fig. 7a the net Hα EW emission in 1994 shows an increase from the beginning of the transit of the hotter component over the cool star disk up to the centre of the secondary (annular) eclipse with a wide plateau centred at phase 0.5. The two 1997 data just outside the secondary eclipse and near the center of the transit seem to show the same behaviour. The observed EW increase at secondary eclipse phases could be simply explained by the decrease of the continuum light due to the eclipse if the active emitting region on the K0 star is not eclipsed. In fact at phase equal to 0.5 ("annularity") the luminosity in V band is about 73% of the luminosity just outside the secondary eclipse (Lanza et al. 1998). Extrapolating this factor to 6563 Å by means of the black-body approximation, we obtain about 72%. Let us define the combined net Hα equivalent width outside eclipse as

$$W_{\rm H\alpha} = \frac{I^1_{\rm H\alpha} + I^2_{\rm H\alpha}}{I^1_{\rm C} + I^2_{\rm C}} = \frac{I^{tot}_{\rm H\alpha}}{I^{tot}_{\rm C}} \quad (4)$$

where $I_{H\alpha}$ is the Hα emission integrated intensity and I_C is the continuum intensity at 6563 Å.

Since our spectra are normalised to the observed continuum, if no active region of the cool star is eclipsed ($I^{tot}_{\rm H\alpha}$ does not change), at the center of the secondary eclipse Eq. (4) becomes

$$W'_{\rm H\alpha} = \frac{I^{tot}_{H\alpha}}{0.72 \cdot I^{tot}_{\rm C}} = 1.39 \cdot W_{\rm H\alpha} \quad (5)$$

Vice-versa, if some emitting region is occulted we should observe a decrease of the Hα equivalent width, while in the case of a homogeneous chromosphere the $W_{\rm H\alpha}$ should remain unchanged. Our 1994 data lead to a value of about 0.22 Å just outside the secondary eclipse and to $\simeq 0.34$ Å near the eclipse center for the Hα emission EW, with a variation of a factor $\simeq 1.54$, that is close to the factor 1.39 of Eq. (5). Thus, taking also into account the estimated errors, the increase we observed in 1994 suggests that no significant part of the active regions has been occulted. The explanation of this behaviour could be that the emitting region is located at high latitudes or, otherwise, that it is extended over the receding limb of the K0 star disk. The lack of observations at the eclipse egress, a situation in which such an extended region would be partially occulted, prevents us from discriminating between these two possibilities.

However it appears that in 1994 there was not a particularly bright emitting region in the inner hemisphere of the cool component occulted during the transit.

6.3. The Hα flare on the cool component of AR Lac

In spite of the lower spectral resolution used in 1989 and 1990, the Hα lines of the two components are well separated on the spectra taken close to the quadratures. This circumstance has allowed us to ascertain that the flare event, detected on September 28 and 29 1989, occurred on the K0 IV component. The short orbital period of AR Lac combined with the daytime interruption of the observations prevented us from accurately determining the time scales of the phenomenon, whose temporal evolution is shown in Fig. 5.

However, we can say that the flare had already begun at JD 2447798.4 (September $28^{\rm th}$) while it was not yet started on September $26^{\rm th}$, when the star was showing the same hemisphere to the observer as at the flare peak. On September $29^{\rm th}$ the flare was still visible although the star was showing the opposite hemisphere of the day before. In September $30^{\rm th}$ the star had already come back to its quiescent level. Therefore, the end and the beginning of the phenomenon are determined with an accuracy of half a day, leading to a duration of 3.0 ± 0.5 days.

Since the flare was observed at opposite phases near quadratures (0.2 and 0.7), its location on the K0 IV can be either at high latitudes or close to the line joining the two components. The spectra observed near phase 0.75 show the Hα line of the K0 IV strongly filled-in by blue-shifted emission, while during the flare decay, at the other quadrature, the filling seems less asymmetrical, but a bit red-shifted. This suggests that the flaring area is located on the hemisphere far from the companion. The change of asymmetry in the emission-line component rules out the possibility of the flare location "above" the star, i.e. near the polar regions.

Several flare events have been observed on AR Lac in various spectral regions from radio (Rodonò et al. 1984) to X-ray (Ottmann & Schmitt 1994, Rodonò et al. 1999) including UV and EUV chromospheric and transition region lines (e.g. Neff et al. 1989, Walter 1996). The flare time-scales generally range from a few hours to a few tens of hours. The long-lasting X-ray flare observed by Ottmann & Schmitt (1994) had a total duration of about $20^{\rm h}$, including two small events during the decay phase. Moreover, the typical flare light curve was followed by a long-duration enhanced emission, lasting more than one orbital period.

We have not enough time resolution to distinguish between a single event or a multiple event, however the light curve behaviour and the changes of the emission line asymmetry suggest a single event or more events from a unique flaring area. Although the rotation could have produced the occultation of some part of the emitting region, modifying the observed temporal trend, we have estimated the energy released, integrating the temporal profile of the Hα luminosity above the solid line showed in Fig. 5, which has been assumed as the quiescent level.

First, we computed the Hα flux at the Earth $f_{H\alpha} = {\rm W}_{\rm H\alpha} \times f_{6563}$, where the flux of the whole system at the Hα continuum, f_{6563} is scaled from the observed V magnitude through the spectrophotometric atlas of Gunn & Stryker (1983) accounting for the contribution of the two components to the total flux, and then we converted it into luminosity adopting the Hipparcos (1997) distance of 42 pc. We have obtained a total energy of about 1.0×10^{35} erg released in the Hα, that must be considered a lower limit not too far from the true value.

In order to make an estimate of the energy budget and to have a guess of the size of the magnetic structure involved, we have used the model proposed by Van den Oord (1988) in which magnetic configurations, significantly influenced by the presence of a close companion are considered. The model is

based on the equilibrium configuration of a straight filament under the Lorentz forces due to the background and/or active region magnetic field, the field produced by the "mirror" surface currents, and the gravitational field.

In a binary system, the current-carrying filament, whose instability may produce the flare, can be placed between the two components. In this case, according to Van den Oord (1988), the maximum energy stored in the filament before it becomes unstable is given by

$$W = 8\,10^{37}\,(\frac{L}{R_\odot})(\frac{a}{R_\odot})^2(\frac{B_{\rm surf}}{1000G})^2\,{\rm erg}. \quad (6)$$

where $2L$ is the filament length, a is the separation of the binary components and $B_{\rm surf}$ is the surface field strength. Kopp & Poletto (1984) showed that, in a strong two-ribbon solar flare, only a fraction of about 0.003 of the magnetic energy stored in the active region heats the plasma. Considering also that roughly one third of the thermal energy of the plasma is lost in the Hα, from the radiative losses observed in Hα we can estimate a total energy budget of the filament of $\sim 10^{38}$ erg. Assuming $B_{\rm surf} = 1000\,{\rm G}$ as a typical value and a filament length equal to the stellar radius, $R_* = 2.66\,R_\odot$, from Eq. (6) we obtain a total stored energy $W \sim 2.2 \times 10^{40}$ erg, i.e. 2 orders of magnitude larger than the stored energy estimated from our observations. Therefore, it seems unlikely to suppose that a large inter-system filament could be responsible for the flare eruption. The observed amount of released energy points toward a smaller structure linked to the cooler star and presumably not influenced by the G2 star, in agreement with a flare located on the far hemisphere of the cool component, as suggested by the changes of the Hα line asymmetry.

In this case we can apply the equation derived for the energy budget of a flare in a single star (see Doyle et al. 1989)

$$W_{single} = 1.6 \cdot 10^{37}(\frac{L}{R_\odot})(\frac{{R_*}^2}{R_\odot})(\frac{B_{surf}}{1000G})^2\,erg \quad (7)$$

where $2L$ is again the filament length, R_* is the radius of the star, and B_{surf} is the surface field strength. Starting with the observed flare energy and $B_{surf} = 1000G$ we obtain $2L \approx 1.3R_\odot$, equal to about $0.4R_*$, a value that, if taken in units of the star radius, is comparable to the typical relative dimensions of solar filaments whose disruption gives rise to the strongest (two-ribbon) flares.

As already found by Catalano & Frasca (1994) for HK Lac, the large energy release, during strong flares in RS CVn system, does not seem to depend on the binary interaction, but it appears to be only related to the size of the magnetic structures involved in such lower gravity stars. It is interesting to note that the geometrical lengths of these filaments, if scaled to the stellar radii, are similar to those of the major solar flares, suggesting that a common scaling law is at work.

7. Conclusion

Our observations of AR Lac have revealed a moderate Hα emission from both components over a large time span from 1989 to 1997. The EW of the average net emission the G2 component is nearly constant through all the observing period and shows a spread compatible with the observational error. The emission of the K0 component shows a spread significantly larger than the error with no particular trend in the different years, indicating a more active chromosphere. The absence of emission noted by Bopp & Talcott (1978) and Huenemoerder & Ramsey (1984) indicates that the system goes through phases of low chromospheric activity as found also from the spots filling factor (Lanza et al. 1998). However it is not clear if the enhanced emission is in phase with the spot coverage. Actually the low emission states found by Bopp & Talcott (1978) and by Huenemoerder & Ramsey (1984) occur just at the beginning and ending of spot maximum, while our observations span from 1989 to 1997, i.e. around the spot minimum to the maximum.

Rotational modulation of Hα emission is generally observed in RS CVn systems (Bopp & Talcott 1978, Ramsey & Nations 1984, Frasca et al. 1996). Moreover, Catalano et al. (1996, 2000) have shown that the Hα emission modulation is usually in antiphase with the photometric wave. However, no clear rotational modulation is detectable in the present Hα emission data of AR Lac.

The most outstanding result of the present Hα investigation is the presence of absorbing material seen just before and during the primary eclipse. The extra absorption in the Hα profile is observed through all the 1997 observations but is absent in 1994 spectra. The absorbing structure seems more likely to be a quasi-static loop anchored on the leading side of the K0 VI component with moderate mass motion inferred from the velocity span of the extra absorption profile. We would like to remark that such prominence-like structures, persisting for several orbital periods in many RS CVn systems (Hall & Ramsey 1992), seem to be always located on the leading hemisphere of the cooler component, or, possibly on the far side with respect to the companion. Whether the formation of such big loops is simply the result of the magnetic activity or the magnetic field just confines in such structures out-flowing matter in the early stage of mass transfer, is at the present not clear.

In 1989 we detected one strong flare implying a total energy release of 10^{35} ergs in the Hα and a storing filament structure of about 0.4 R_* located in the external hemisphere of the K star.

From our new radial velocity measurements, the solution of the orbital elements gives a slight difference between the masses of the two components in better agreement with their spectral type and luminosity class, i.e. evolutionary path.

We have discussed here the Hα emission behaviour of AR Lac on a long time scale, but the data obtained in 1997 will be further discussed in a subsequent paper dedicated to a multi-wavelength study including the coordinated observations with the X-ray satellite Beppo-SAX, the VLA and VLBA radio observations, and optical photometry.

Acknowledgements. The authors are very grateful to Dr. A.F. Lanza for a critical reading of the paper and interesting discussions. We would like to thank an anonymous referee for useful suggestions. This work has been supported by the Italian *Ministero dell' Università e della Riscerca Scientifica e Tecnologica*, the *Gruppo Nazionale di Astronomia* of the

CNR and by the *Regione Sicilia* which are gratefully acknowledged. This research has made use of the ADS-CDS databases, operated at the CDS, Strasbourg, France.

References

Al-Naimiy H.M., 1978, Ap&SS 53, 181
Barden S.C., 1985, ApJ 295, 162
Bopp B. W., 1983, In: P.B. Byrne and M. Rodonò (eds.), Activity in Red Dwarf Stars, Proc. IAU Coll. No. 71, Dordrecht: Reidel, p. 363
Bopp B.W., Talcott J.C., 1978, AJ 83, 1517
Bopp B.W., Talcott J.C., 1980, AJ 85, 55
Catalano S., Frasca A., 1994, A&A 287, 575
Catalano S., Rodonò M., Frasca A., Cutispoto G., 1996, In: K.G. Strassmeier and J. Linsky (eds.), Stellar Surface Structure, Proc. IAU Symp. No. 176, p. 403
Catalano S., Rodonò M., Cutispoto G., Frasca A., 2000, In: C. İbanoğlu (ed.), Variable Stars as Essential Astrophysical Tools. Kluwer Academic Publisher, p. 687
Cram L.E., Mullan D.J., 1985, ApJ 294, 626
Doyle J. G., Byrne P. B., Van den Oord G. H. J., 1989, A&A 224, 153
ESA, 1997, The Hipparcos and Tycho Catalogues. ESA SP-1200
Evans D.S., 1967, in: A.H. Batten, J.F. Heard (eds.), Determination of Radial Velocities and their Applications. Proc. IAU Symp. No. 30. Academic Press, p. 57
Feldman P.A., 1978, BAAS 10, 418
Fernańdez-Figueroa M.J., Montes D., De Castro E., Cornide M., 1994, ApJS 90, 433
Fitzpatrick M.J., 1993, In: R.J. Hanish, R.V.J. Brissenden, J. Barnes (eds.), Astronomical Data Analysis Software and Systems II, PASPC 52, 472
Frasca A., Catalano S., 1994, A&A 284, 883
Frasca A., Catalano S., Marilli E., 1996, In: Y. Uchida, H.S. Hudson, T. Kosugi (eds.), Magnetodynamic Phenomena in the Solar Atmosphere. Prototypes of Stellar Magnetic Activity. Proc. IAU Coll. No. 153, Kluwer Scientific Publishers, 475
Griem H.R., 1962, ApJ 136, 422
Gray D.F., 1992, The Observation and Analysis of Stellar Photospheres, Cambridge University Press
Guinan E.F., Wacker S.W., Baliunas S.L. et al., 1986, in: New Insights in Astrophysics. ESA SP-263, p. 197
Gunn A.G., Hall J.C., Lockwood G.W., Doyle J.G., 1996, A&A 305, 146
Gunn A.G., Mitrou C.K., Doyle J. C., 1998, MNRAS 296, 150
Gunn J., Stryker L.L., 1983, ApJS 52, 121
Hall J.C., Huenemoerder D.P., Ramsey L.W., Buzasi D.L., 1990, ApJ 358, 610
Hall J.C., Ramsey L.W., 1992, AJ 104, 1942
Hall J.C., Wolowitz J.B., 1998, ApJ 115, 2571
Harper W.E., 1933, J. R. Astron. Soc. Can. 27, 146
Herbig G.H., 1985, ApJ 289, 269
Huenemoerder D.P., Ramsey L.W., 1984, AJ 89, 1984
Kopp R.A., Poletto G., 1984, Solar. Phys. 93, 351
Lanza A.F., Catalano S., Cutispoto G., Pagano I., Rodonò M., 1998, A&A, 332, 541
Lefèvre E., Klein K.L., Lestrade J.F, 1994, A&A, 483
Liu X., Tan H., 1986, Chin. Astron. Astrophys. 10, 221
Marino G., Catalano S., Frasca A., Marilli E., 1998, IBVS 4599
Montes D., Fernańdez-Figueroa M.J., De Castro E., Cornide M., 1995, A&A 294, 165
Montes D., Fernańdez-Figueroa M.J., De Castro E., Sanz-Forcada J., 1997, A&AS 125, 263
Moore C.E., Minnaert M.G.J., Houtgast J., The Solar Spectrum 2935 Å to 8770 Å, 1966, US Dept. of Commerce, Monograph 61
Nations H.L., Ramsey L.W., 1980, AJ 85, 1086
Neff J.E., 1992, in: P.B. Byrne, D.M. Mullan (eds.), Surface Inhomogeneities on Late-Type Stars. Berlin: Springer-Verlag, p. 54
Neff J.E., Walter F.M., Rodonò M., Linsky J.L., 1989, A&A 215, 79
Ottmann R., Schmitt J.H.M.M., Kürster M., 1993, ApJ 413, 710
Ottmann R., Schmitt J.H.M.M., 1994, A&A 283, 871
Pagano I., 1990, Degree Thesis, Univ. of Catania
Pagano I., 1993, PhD Thesis, Univ. of Catania
Pagano I., Rodonò M., Neff J.E., Walter F.M., 1994, In: Caillault J-P. (ed.), Cool Stars, Stellar Systems, and the Sun. 8th Cambridge Workshop. ASP Conf. Series 64, p. 450
Pasquini L., Pallavicini R., 1991, A&A 251, 199
Popper D.M., 1980, ARA&A, 18, 115
Popper D.M., 1990, AJ, 100, 247
Rodonò M., Cutispoto G., Catalano S., et al., 1984, Proc. 4th European IUE Conference, ESA, SP-218, 247
Rodonò M., Pagano I., Leto G., et al. 1999, A&A 346, 811
Ramsey L.W., Nations H. L., 1984, AJ 89, 115
Sanford R.F., 1951, ApJ 113, 299
Siarkowski M., Preś P., Drake S.A., White N.E., Singh K.P., 1996, ApJ 473, 470
Simkin S.M., 1974, A&A 31, 129
Strassmeier K.G., Fekel F.C., Bopp B.W., et al. 1990, ApJS 72, 191
Strassmeier K.G., Hall D.S., Fekel F.C., Scheck M., 1993, A&AS 100, 173
Tonry J., Davis M., 1979, AJ 84, 1511
Van den Oord G.H.J., 1988, A&A 205, 167
Walter E.J., Gibson D.M., Basri G., 1983, ApJ 267, 665
Walter F.M., 1996, in: S. Bowyer, R.F. Malina (eds.), Astrophysics in the Extreme Ultraviolet. Kluwer Academic Publisher, p. 129
White N.E., Shafer R.A., Horne K., Parmar A.N., Culhane J.L., 1990, ApJ 350, 776
White N.E., Arnaud K., Day C.S.R., et al., 1994, PASJ 46, L97